BIOLOGICAL CRYSTALLOGRAPHY

ISSN 1399-0047

A conformational change in the peripheral anionic site of *Torpedo californica* acetylcholinesterase induced by a bis-imidazolium oxime

Patricia M. Legler,[a]* Iswarduth Soojhawon[b] and Charles B. Millard[c]‡

[a]CBMSE, U.S. Naval Research Laboratory, 4555 Overlook Avenue, Washington, DC 20375, USA, [b]Bacterial Diseases, Walter Reed Army Institute of Research, 503 Robert Grant Avenue, Silver Spring, MD 20910, USA, and [c]Division of Biochemistry, Walter Reed Army Institute of Research, 503 Robert Grant Avenue, Silver Spring, MD 20910, USA. *Correspondence e-mail: patricia.legler@nrl.navy.mil

Received 6 May 2015
Accepted 9 June 2015

Edited by Z. S. Derewenda, University of Virginia, USA

‡ Current address: 176 Thomas Johnson Drive, Suite 105, Frederick, MD 21702, USA.

Keywords: acetylcholinesterase; peripheral anionic site; allosterism; oxime; organophosphate.

PDB references: TcAChE, complex with 2BIM-7, 5bwb; complex with Ortho-7, 5bwc

Supporting information: this article has supporting information at journals.iucr.org/d

As part of ongoing efforts to design improved nerve agent antidotes, two X-ray crystal structures of *Torpedo californica* acetylcholinesterase (*Tc*AChE) bound to the bis-pyridinium oxime, Ortho-7, or its experimental bis-imidazolium analogue, 2BIM-7, were determined. Bis-oximes contain two oxime groups connected by a hydrophobic linker. One oxime group of Ortho-7 binds at the entrance to the active-site gorge near Trp279, and the second binds at the bottom near Trp84 and Phe330. In the Ortho-7–*Tc*AChE complex the oxime at the bottom of the gorge was directed towards the nucleophilic Ser200. In contrast, the oxime group of 2BIM-7 was rotated away from Ser200 and the oxime at the entrance induced a significant conformational change in the peripheral anionic site (PAS) residue Trp279. The conformational change alters the surface of the PAS and positions the imidazolium oxime of 2BIM-7 further from Ser200. The relatively weaker binding and poorer reactivation of VX-inhibited, tabun-inhibited or sarin-inhibited human acetylcholinesterase by 2BIM-7 compared with Ortho-7 may in part be owing to the unproductively bound states caught *in crystallo*. Overall, the reactivation efficiency of 2BIM-7 was comparable to that of 2-pyridine aldoxime methyl chloride (2-PAM), but unlike 2-PAM the bis-imidazolium oxime lacks a fixed charge, which may affect its membrane permeability.

1. Introduction

Acetylcholinesterase (AChE; EC 3.1.1.7) is an α/β-hydrolase known best for its primary role of catalyzing hydrolysis of the neurotransmitter acetylcholine (ACh) with remarkable efficiency at the neuromuscular junction. The enzyme contains a deep, narrow, hydrophobic gorge leading to a Ser/His/Glu catalytic triad at the bottom (Sussman *et al.*, 1991, 1993; Fig. 1*a*). At the top of the gorge, AChE has a conserved binding site known historically as the 'peripheral anionic site' (PAS) that has been well described topographically and shown to function as an allosteric effector site for binding ACh and other small molecules that modulate esterase activity (Rydberg *et al.*, 2006). The residues of the PAS are more aromatic than anionic and consist of Tyr70, Asp72, Tyr121, Trp279 and Tyr334 in *Torpedo californica* AChE (*Tc*AChE) or Tyr72, Asp74, Tyr124, Trp286 and Tyr341 in human AChE. Despite an overall sequence homology with AChE of greater than 50%, the residues of the PAS are not conserved in human butyrylcholinesterase (BChE; EC 3.1.1.8). In several X-ray crystal structures, binding events at the PAS have been linked to conformational changes at the enzyme active site ~20 Å away. Binding of aflatoxin at the periphery, for example, leads

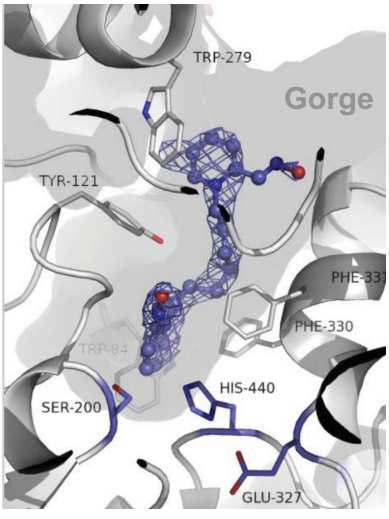

© 2015 International Union of Crystallography

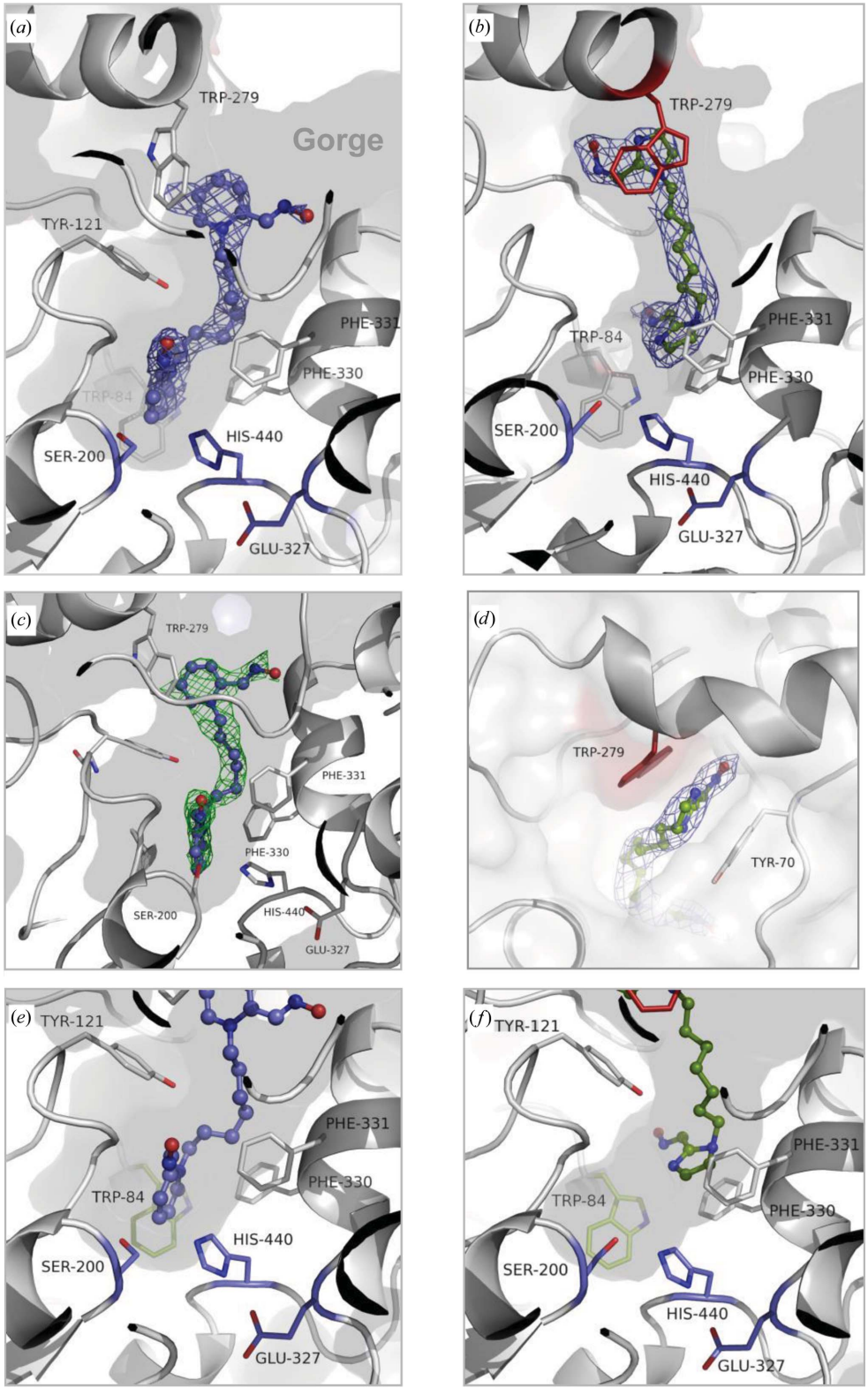

Figure 1
Comparison of bis-pyridinium and bis-imidazolium oxime-bound structures. (*a*) Ortho-7 (PDB entry 5bwc) and (*b*) 2BIM-7 (PDB entry 5bwb) bound to *Tc*AChE. The fitted electron density is shown. The catalytic triad (Ser200/His440/Glu327) at the bottom of the gorge is shown in blue. Trp279 (colored red) undergoes a conformational change at the top of the gorge when 2BIM-7 is bound. (*c*) $F_o - F_c$ maps of Ortho-7. (*d*) 2BIM-7 stacks face-to-face with Trp279 of the allosteric peripheral anionic site and Tyr70. (*e*) At the bottom of the gorge Ortho-7 is well aligned for attack. The edge of the Ortho-7 pyridinium ring interacts with the face of Trp84 (colored green; Brocchieri & Karlin, 1994). (*f*) in contrast, 2BIM-7 is rotated away from the active-site serine and the edge-to-face interaction with Trp84 is lost.

to the opening of a 'back door' and access to the active site at the bottom of the gorge (PDB entry 2xi4; Sanson *et al.*, 2011; Gilson *et al.*, 1994). Conversely, covalent reaction of Ser200 with diisopropyl fluorophosphate (DFP) at the bottom of the gorge (PDB entry 2dfp; Millard *et al.*, 1999) leads to a conformational change in the loop containing PAS residue Trp279 at the top of the gorge. Several other molecules bind to the PAS and induce conformational changes in Trp279 directly, *e.g.* NF595 (PDB entry 2cek; Colletier *et al.*, 2006) and TZ2PA6 (PDB entry 1q83; Bourne *et al.*, 2004). While these X-ray studies suggest that the PAS can serve as an alternate site for the rational design of allosteric drugs (Johnson & Moore, 2006), further work is required to understand the coordinated motions of ligand-induced conformational changes.

Organophosphate (OP) nerve agents such as VX, soman (GD) or sarin (GB) react with the active-site Ser200 and covalently inhibit AChE (Supplementary Scheme S1). Inhibition results in the rapid accumulation of ACh at the neuromuscular junction (NMJ), as well as at nerve–nerve synaptic clefts, and may lead to cholinergic crisis, including convulsions, respiratory paralysis and death. Nucleophilic attack at the phosphorus-serinyl adduct by small-molecule oxime antidotes has been the predominant therapeutic strategy for restoring AChE activity. Most therapeutic oximes either bind in the active site, where they align for direct attack at the phosphorus, or bind at the PAS and extend a reactive nucleophile down the gorge to reach the OP adduct (Luo *et al.*, 2010; Wilson & Ginsburg, 1955); bis-oximes exploit binding at both sites (Hammond *et al.*, 2003; Pang *et al.*, 2003; Ekström *et al.*, 2006; Fig. 1). While thousands of oximes have been tested in the

literature, 2-pyridine aldoxime methyl chloride (2-PAM) remains the clinical standard and is stockpiled as an OP antidote in the United States (Broach *et al.*, 2014; Burda & Sigg, 2001). Several promising bis-oximes, including obidoxime (toxogonin), TMB-4 (trimedoxime bromide), MMB-4 (1,1-methylene bis{4-[(hydroxyimino)methyl]-pyridinium} dibromide) and HI-6 [1-({[4-(aminocarbonyl)-pyridinio]methoxy}methyl)-2-[(hydroxyimino)methyl]pyridinium chloride], are in use or development worldwide (reviewed in Hammond *et al.*, 2003; Worek & Thiermann, 2013). Each oxime is optimal against a different set of OP–AChE adducts and there is currently no universally effective oxime antidote against all known nerve agents and OP pesticides (Jokanović & Prostran, 2009). Oxime reactivation of soman–AChE and tabun (GA)–AChE conjugates remains especially challenging (Worek & Thiermann, 2013). Moreover, drug penetration across the blood–brain barrier (BBB) to reactivate central nervous system AChE is poorly achieved by existing oximes. The development of BBB-permeable oximes, and oximes or small molecules able to reactivate dealkylated (aged) OP–AChE adducts, is still in its infancy (Mercey *et al.*, 2012; Steinberg *et al.*, 1970; Wandhammer *et al.*, 2013).

One promising bis-oxime, Ortho-7 (Fig. 2), was able to partially reactivate mouse AChE *in vitro* following inhibition with tabun (Ekström *et al.*, 2006), echothiophate (an FDA-approved glaucoma therapeutic that is structurally similar to VX) and DFP (Pang *et al.*, 2003). To improve upon this preliminary result, we designed and synthesized stable bis-imidazolium oximes with a reduced volume to promote better alignment and reduced steric hindrance in the narrow gorge. The gorge can be partially occluded by OPs carrying bulky alkyl groups, and optimal alignment for nucleophilic attack by oximes can be hindered (Jokanović & Prostran, 2009; Jokanović, 2012; Stojiljković & Jokanović, 2006). The novel oxime series with variable alkyl linkers was denoted '2BIM'.

Here, we report the kinetic and structural characterization of this novel class of compounds. The structure of *Tc*AChE–2BIM-7 (PDB entry 5bwb) is the first published crystal structure of a bis-imidazolium oxime bound to a cholinesterase and reveals that the oxime binds away from the active-site serine and induces rotation of a key PAS residue, Trp279, which alters the entrance to the gorge. We also present the structure of a bis-pyridinium oxime, Ortho-7, bound to *Tc*AChE (PDB entry 5bwc) and compare it with a previously

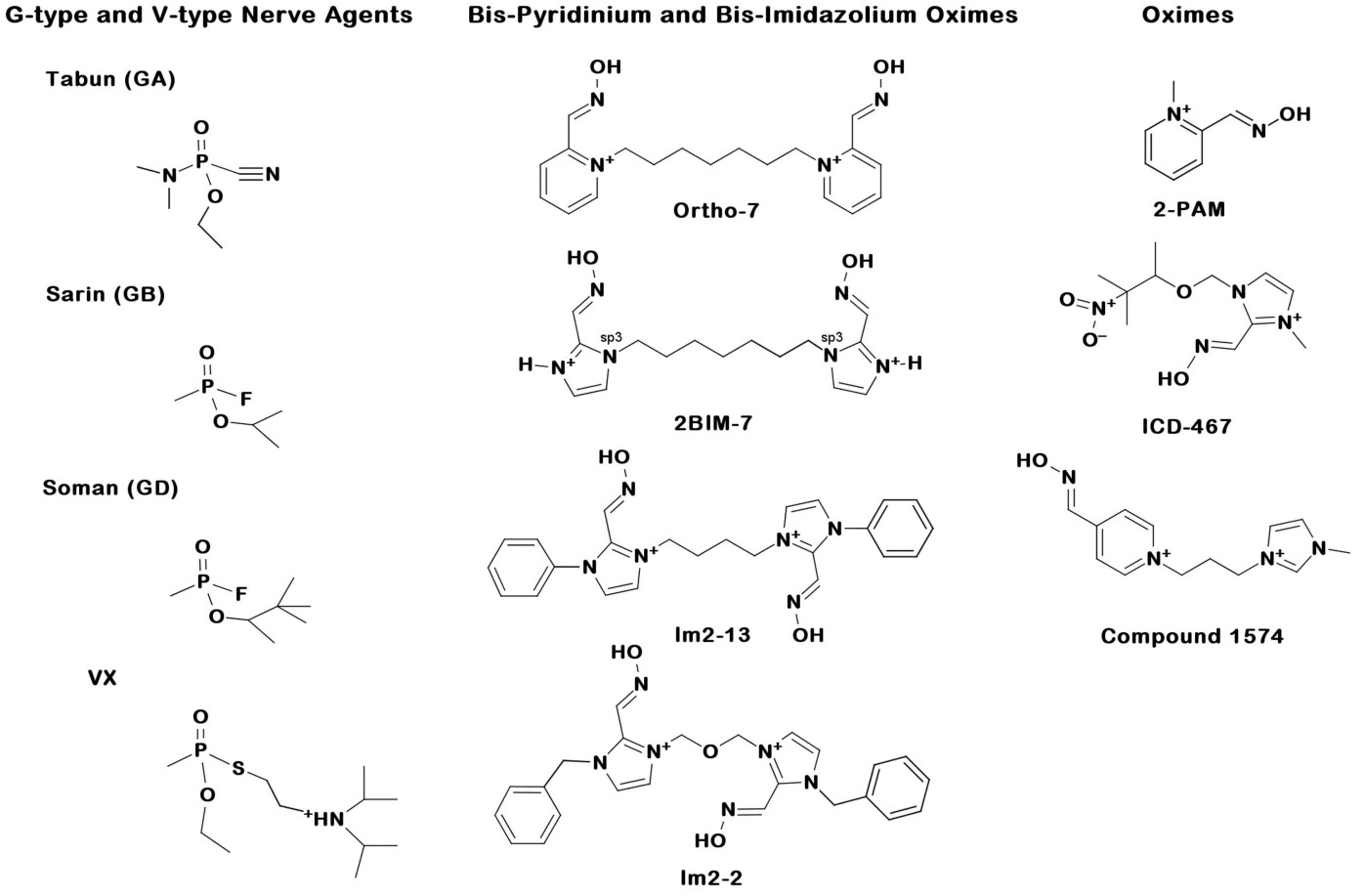

Figure 2
Structures of G-type and V-type nerve agents and bis-pyridinium and bis-imidazolium oximes. The ring N atom attached to the linker in 2BIM-7 is sp^3-hybridized and has tetrahedral geometry in the X-ray crystal structure, indicating that the lone pair is predominantly present on this nitrogen. The pyridinium-ring N atom of Ortho-7 is sp^2-hybridized (planar) in the X-ray crystal structure. Crystal structures of the other oximes shown have not been determined.

determined structure of a mouse AChE (mAChE)–Ortho-7 complex (PDB entry 2gyv; Ekström *et al.*, 2006). The orientation of the oxime at the bottom of the gorge appears to correlate with the conformer of Trp279 at the top of the gorge. The conformational changes are consistent with an allosteric mechanism involving binding at the PAS and may have implications for how we assess the long-term and short-term effects of oxime reactivators and anticholinesterase compounds which cross the BBB.

2. Materials and methods

2.1. Purification of *Tc*AChE

Purification of *Tc*AChE was carried out by an affinity-chromatography procedure, subsequent to its solubilization by phosphatidylinositol-specific phospholipase C (PI-PLC, Sigma) as described previously (Millard *et al.*, 1999; Sussman *et al.*, 1988). All chemicals were purchased from Sigma (St Louis, Missouri, USA). *T. californica* frozen electric organ was purchased from Aquatic Research Consultants (San Pedro, California, USA). Briefly, frozen electric organ was homogenized in 10 m*M* Tris–HCl pH 8.0, 100 m*M* NaCl and incubated with PI-PLC (1 µg ml^{-1}) for 18 h at room temperature. The tissue was separated by ultracentrifugation and the supernatant was then loaded onto an affinity column [conjugated with *m*-(aminophenyl)trimethylammonium]. Bound *Tc*AChE was eluted from the column with 49 m*M* tetramethylammonium bromide in the same buffer. Purified acetylcholinesterase was dialyzed extensively against 10 m*M* 2-(*N*-morpholino)ethanesulfonic acid (MES) buffer pH 6.5, 100 m*M* NaCl. The purity of *Tc*AChE was determined by SDS–PAGE.

2.2. Co-crystallization, X-ray diffraction and data processing

Protein at approximately 12–14 mg ml^{-1} was mixed in a 1:1 ratio with the precipitant [36%(*w*/*v*) PEG 200 in 0.2 *M* MES buffer pH 5.7–6.0] at 4°C. Crystals of *Tc*AChE were soaked with Ortho-7 (19.2 m*M*) for 1 d at 4°C. The bis-imidazolium oxime, 2BIM-7, and the bis-pyridinium oxime, Ortho-7, were a kind gift from Dr Yuan-Ping Pang at Mayo Clinic, Rochester, Minnesota, USA. Crystals of *Tc*AChE bound to 2BIM-7 were obtained by co-crystallization (1 m*M* 2BIM-7) followed by soaking (20 m*M*) for 6 d. Crystals were looped in Paratone-N and flash-cooled in liquid nitrogen. Data were collected at 100 K on a Bruker FR591 high-flux, rotating-anode X-ray diffractometer using a SMART 6000 2K CCD detector. Initial phases were calculated from PDB entry 2ace (Raves *et al.*, 1997), and the structures were determined by molecular replacement using *AMoRe* (Navaza, 2001). Models were refined using *REFMAC*5 (Winn *et al.*, 2011) and simulated annealing was performed using *CNS* (Brünger *et al.*, 1998). Models were manipulated with *Coot* (Emsley & Cowtan, 2004). Oxime coordinates and topology files were created using the *PRODRG*2 server (Schüttelkopf & van Aalten, 2004).

2.3. Enzyme assays and preparation of non-aged sarin, tabun and VX conjugates of AChE

Human AChE (huAChE) was a kind gift from Dr Nageswararao Chilukuri (USAMRICD, Aberdeen Proving Ground, Edgewood, Maryland, USA). Enzyme activity was determined using the method of Ellman (Ellman & Lysko, 1979). The assay mixture consisted of 0.75 m*M* acetylthiocholine, 1.0 m*M* DTNB in 50 m*M* Sorensen buffer pH 7.4. All measurements were performed at 23 ± 2°C in 1.5 ml cuvettes.

Non-aged GA, GB and VX conjugates of AChE were prepared in 100 m*M* TAPS buffer pH 9.5 according to Luo *et al.* (2010) to minimize the 'aging' process of the nerve-agent conjugates of the enzyme. Briefly, 10–100 µl of 4000 U huAChE or *Tc*AChE was incubated with a small volume (2–10 µl) of 100 µ*M* organophosphate (GA, GB or VX) for 30 min at room temperature to achieve 96–98% inhibition. Excess organophosphate was either removed by passing the solution through a PD-10 column (GE Healthcare) or by adding fresh enzyme to the GA-, GB- or VX-inhibited sample. The absence of inhibitory activity was confirmed by incubation of the non-aged nerve agent-inhibited samples with fresh huAChE for 30 min at 25°C and pH 7.4. No inhibition of the fresh enzyme was observed. The non-aged GA-, GB- or VX-inhibited sample was then diluted tenfold in 100 m*M* TAPS buffer pH 9.5 and stored at −20°C in 50% glycerol until use (Luo *et al.*, 2010).

2.4. Reactivation of organophosphate-inhibited AChE

Reactivation rates were measured discontinuously so that higher oxime concentrations of up to 5 m*M* could be tested (Wang & Braid, 1967). A 20-fold dilution of the OP-inhibited conjugate of huAChE was incubated with various concentrations of oximes at 25°C for 15 min. At specific time intervals, aliquots (20–100 µl) of the reactivation product were transferred to a cuvette containing 900 µl assay mixture and product formation was monitored at 412 nm for 1 min. Between five and ten different oxime concentrations ranging from 0.1 to 2000 µ*M* were evaluated. Enzyme activities were corrected for the reaction of the oximes with the substrate.

2.5. Kinetics of oxime reactivation

Oxime reactivation of AChE inhibited by an OP can be described by (1), where EP represents the phosphorylated enzyme; Ox the oxime; (EP • Ox) is a Michaelis-type complex formed by the phosphorylated enzyme and the oxime; E is the reactivated enzyme and P-Ox is the phosphylated oxime,

$$\mathrm{EP} + \mathrm{Ox} \overset{K_\mathrm{d}}{\rightleftharpoons} (\mathrm{EP} \bullet \mathrm{Ox}) \overset{k_\mathrm{r}}{\rightarrow} \mathrm{E} + \mathrm{P\text{-}Ox}. \qquad (1)$$

The pseudo-first-order rate constant for reactivation, k_{obs}, was measured for each oxime concentration (Wang & Braid, 1967) using (2), where v_0 is the enzyme activity of the control AChE; v_i is the activity of the phosphorylated AChE; and v_t is the activity of the reactivated AChE at time t,

Table 1
X-ray crystallographic data-collection and refinement statistics.

	*Tc*AChE–Ortho-7	*Tc*AChE–2BIM-7
PDB entry	5bwc	5bwb
Space group	$P3_121$	$P3_121$
Unit-cell parameters (Å, °)	$a = b = 112.15$, $c = 137.33$, $\alpha = \beta = 90.00$, $\gamma = 120.00$	$a = b = 112.30$, $c = 137.11$, $\alpha = \beta = 90.00$, $\gamma = 120.00$
Wavelength (Å)	1.54	1.54
Resolution range (Å)	28.04–2.45 (2.54–2.45)	56.15–2.57 (2.66–2.57)
Unique reflections	37229 (3733)	32414 (3136)
R_{merge}	0.188 (0.457)	0.125 (0.407)
$\langle I/\sigma(I)\rangle$	9.3 (4.1)	17.2 (5.6)
Completeness (%)	99.9 (100.0)	100.0 (100.0)
Multiplicity	8.9 (7.8)	13.6 (13.6)
Refinement statistics		
Resolution (Å)	2.45–28.05	2.57–56.15
No. of reflections	34919	29650
R factor	0.243	0.210
R_{free}	0.266	0.242
No. of atoms		
Total	4411	4515
Protein	4244	4245
Solvent	114	208
Other	52	62
Average *B* factors (Å^2)		
Protein	20.9	33.6
Solvent	14.8	30.4
Other	27.7	45.8
R.m.s.d. from ideal geometry		
Bond lengths (Å)	0.008	0.008
Bond angles (°)	1.29	1.26
Ramachandran plot		
Most favored regions (%)	90.3	90.1
Additional allowed regions (%)	9.5	9.7
Generously allowed regions (%)	0.2 [Ser200†]	0.0
Disallowed regions (%)	0.0	0.2 [Ser200†]

† The nucleophilic serines of serine esterases are found in a sharp turn known as the 'nucleophilic elbow' and are typically in a disallowed or generously allowed region of the Ramachandran plot (Nardini & Dijkstra, 1999).

$$\ln(v_0 - v_t)/(v_0 - v_i) = -k_{obs}t. \quad (2)$$

A plot of $\ln(v_0 - v_t)/(v_0 - v_i)$ against t gave k_{obs} values for each oxime concentration.

K_d is the kinetically determined dissociation constant of the oxime from the phosphylated enzyme. k_r is the reactivation rate constant for the oxime and is the extrapolated value of k_{obs} at infinite oxime concentration. When the oxime concentration equals K_d, $k_{obs} = 0.5k_r$. Both kinetic constants can be determined from measurements of k_{obs} at varying concentrations of oxime [Ox] and a nonlinear fit to (3). A plot of k_{obs} *versus* oxime concentration yields the K_d and k_r values,

$$k_{obs} = k_r[\mathrm{Ox}]/(K_d + [\mathrm{Ox}]). \quad (3)$$

The second-order rate constant k_{r2} is the bimolecular rate constant and reflects the overall reactivating efficiency of the oxime,

$$k_{r2} = k_r/K_d. \quad (4)$$

3. Results

3.1. Ortho-7 binding interactions

The bis-pyridinium oxime Ortho-7 was co-crystallized with *Tc*AChE. X-ray crystallographic data-collection and refinement statistics are shown in Table 1. At the top of the gorge, the oxime is positioned to make π–π and cation–π binding interactions with Trp279 of the PAS, and at the bottom of the gorge Phe330 and Trp84 interact with the second oxime group (*Tc*AChE numbering is used throughout; Figs. 1*a* and 1*e*). At the top of the gorge density for the N—OH group is weak (Fig. 1*a*). This may be owing to either static or dynamic disorder. Notably, at the bottom of the gorge the O atom of the oxime moiety is in line for attack and is 4.5 Å from the nucleophilic serine O$^\gamma$ that becomes phosphylated by OP inhibitors (Fig. 1*e*). We next looked at the conformation of the oxime group at the bottom of the gorge nearest Ser200 to determine whether it was in the *syn*-I, *syn*-II or *anti* conformation (Pang *et al.*, 2003). The *syn*-I conformation was observed at the bottom of the gorge, which is in agreement with a prior prediction based upon density functional theory calculations (Pang *et al.*, 2003). It should be noted that the conformation was observed in the absence of an OP and may or may not be the conformation relevant to reactivation. The biologically active conformation has been debated (Pang *et al.*, 2003); therefore, kinetic parameters were also measured (§3.4).

3.2. 2BIM-7 binding interactions

The bis-imidazolium oxime, 2BIM-7, was also co-crystallized with *Tc*AChE (Table 1). Unlike the bis-pyridinium oxime, the bis-imidazolium oxime has two N atoms in its heterocyclic rings. The ability of bis-imidazolium oximes to reactivate tabun-inhibited AChE was suggested to be owing to their geometry and their ability to access the phosphorus (a smaller five-membered ring *versus* a six-membered ring; Kovarik *et al.*, 2013). Inspection of the electron density shows that the ring N atom attached to the carbon linker in the bis-imidazolium is tetrahedral (sp^3-hybridized; Supplementary Fig. S1, Fig. 1*f*), whereas the ring N atom attached to the carbon linker of the bis-pyridinium oxime Ortho-7 is planar (sp^2-hybridized) and is part of a conjugated system (Figs. 1*c* and 2). The C(linker)—N(sp^3)—C(ring) bond angles in the 2BIM-7 oxime group at the bottom of the gorge were 113 and 114°. The sp^3 hybridization induces a sharp bend between the imidazolium ring and the carbon linker; this may affect the alignment during nucleophilic attack (Supplementary Fig. S1). The other ring N atom of the bis-imidazolium oxime can carry a positive charge (Fig. 2). In the observed conformation, cation–π and π–π stacking interactions are made with Phe330 and Phe331 near the base of the gorge (Fig. 1*f*). The imidazolium oxime is rotated away from Ser200 in an unproductive state, and the O atom of the oxime is 11.4 Å from Ser200 O$^\gamma$. The bis-imidazolium oxime in this conformation is cradled by three residues, Tyr334, Phe330 and Phe331, at the bottom of the gorge. Interestingly, Kovarik and coworkers found that a Y377A mutation enhanced reactivation threefold for some imidazole-containing aldoximes (Kovarik *et al.*, 2013). Tyr337

PDB code	Species	Color	Ligand
1ea5	*T. californica*	Gray	—
1q83	Mouse	Cyan	TZ2PA6
2dfp	*T. californica*	Pink	DFP
2ckm	*T. californica*	Yellow	Bis-tacrine
2cek	*T. californica*	Lime	NF595
1eve	*T. californica*	Gold	Aricept (donepezil)
2vq6	*T. californica*	Orange	2-PAM
2gyv	Mouse	Light purple	Ortho-7
5bwc	*T. californica*	Slate blue	Ortho-7
5bwb	*T. californica*	Red	2BIM-7
1n5r	Mouse	Blue	Propidium
1gqr	*T. californica*	Light blue	Rivastigmine

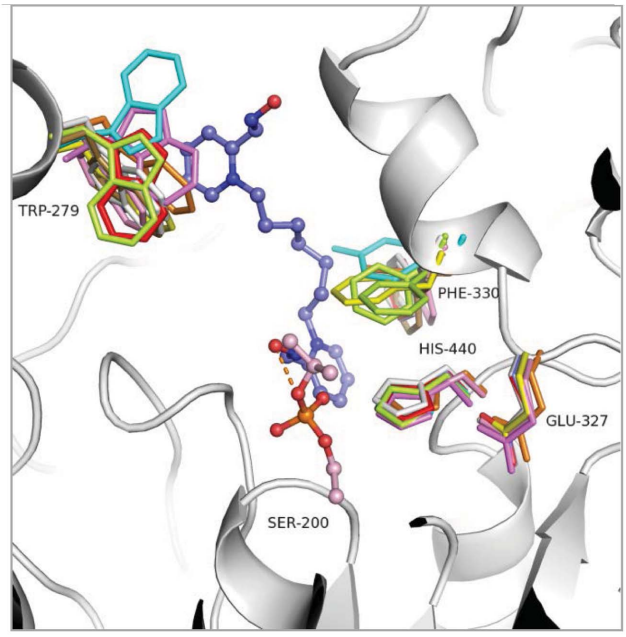

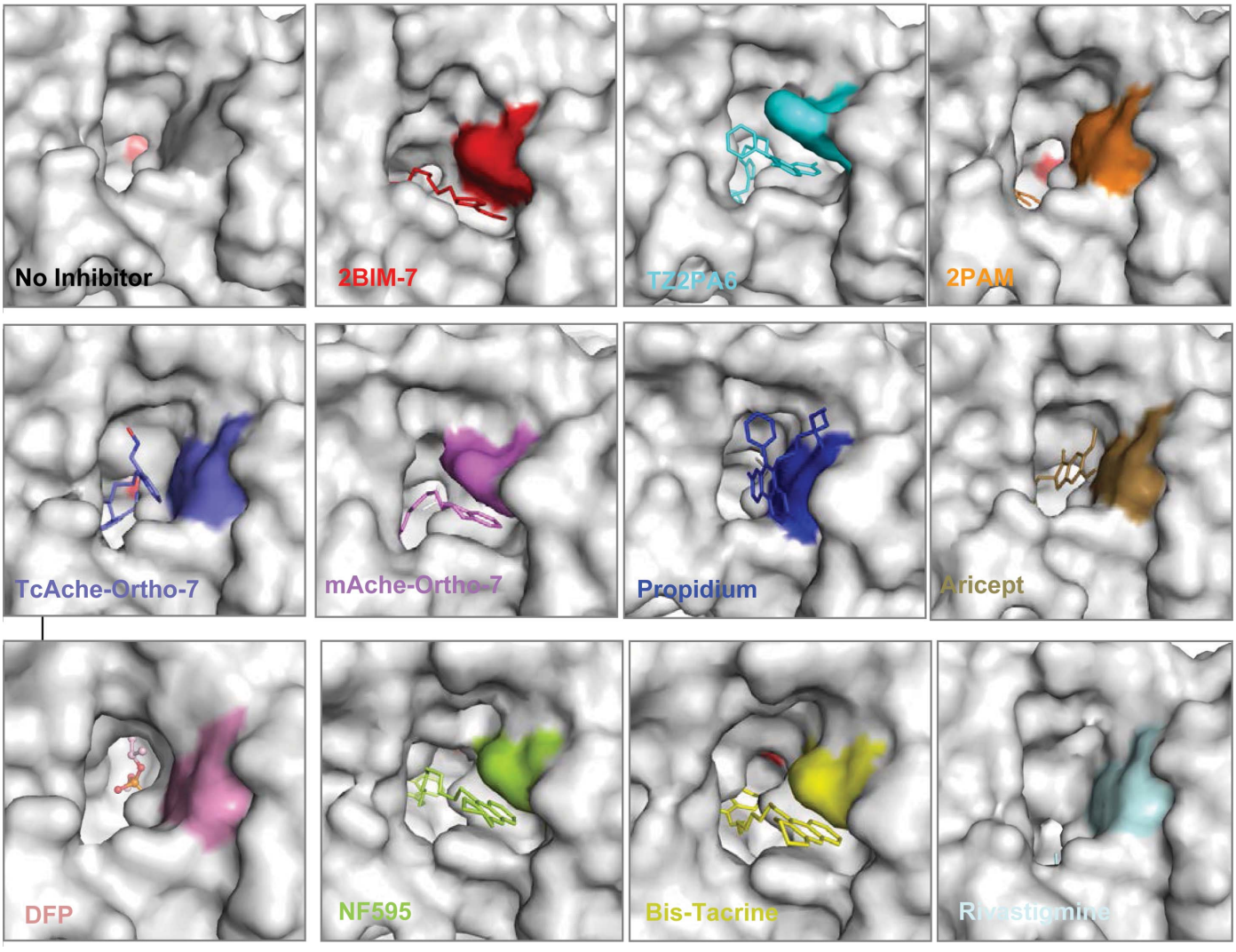

Figure 3
Ligand-induced surface alterations of the PAS. Several compounds have been shown to induce conformational changes in AChE. NF595 induces a conformational change similar to that found in 2BIM-7. The lower panels are views looking down the gorge. Ser200 is at the bottom of the gorge. Trp279 of the PAS is colored. DFP is covalently bound to Ser200 (shown as a sphere).

of human AChE corresponds to Phe330 in *Tc*AChE and Tyr337 in mouse AChE. Phe330 (Tyr337) interacts with the oxime at the bottom of the gorge, which is found in an unproductive conformation in both *Tc*AChE and mouse AChE (*i.e.* the oxime is rotated away from Ser200). The Y377A mutation may lessen these unproductive interactions and account for the previously observed enhancement.

At the top of the gorge, 2BIM-7 induces a significant conformational change in Trp279 (Fig. 1*b*), which effectively alters the surface of the PAS (Fig. 3). The imidazolium ring makes face-to-face interactions with Trp279 and Tyr70 in a relatively flat pocket (Fig. 1*d*). Looking down the gorge, the linker and second oxime group effectively occlude the gorge (Fig. 1*d*) and may prevent subsequent rephosphorylation of the active-site serine. Notably, no significant differences in the catalytic triad residues or oxyanion-hole residues were observed.

3.3. Comparison with other small molecules

Conformational changes in Trp279 have been reported in five other publically available structures of AChE (Rydberg *et al.*, 2006; Millard *et al.*, 1999; Colletier *et al.*, 2006; Bourne *et al.*, 2004; Ekström *et al.*, 2006; Fig. 3). The structure of the 2BIM7–*Tc*AChE complex is the sixth example of a significant small-molecule-induced conformational change in the PAS. The *Tc*AChE PAS is formed by Tyr70, Asp72, Tyr121, Trp279 and Tyr334. The Trp279 conformer observed in the *Tc*AChE complex with 2BIM-7 has also been observed in PDB entry 2cek (Colletier *et al.*, 2006), which is a structure of *Tc*AChE bound to NF595. NF595 is a bifunctional inhibitor similar to the bis-oximes; its binding also induced conformational changes in Phe330 and Phe331. While the conformer of Trp279 is similar in the 2BIM-7 and NF595 complexes, the rotamers of Phe330 differ. In contrast, no significant movement of Phe330 or Phe331 was observed in the 2BIM-7 structure.

The PAS residue Trp279 can be found in one of five conformations. The gorge opening in the structure of the free enzyme is similar to that found in the *Tc*AChE–2PAM, *Tc*AChE–Ortho7, mouse AChE–propidium, *Tc*AChE–donepezil, *Tc*AChE–rivastigmine and *Tc*AChE–DFP structures (Fig. 3). The surface of the PAS changes significantly when 2BIM-7, TZ2PA6, bis-tacrine or NF595 are bound. Interestingly, in the case of Ortho-7, Trp279 is found in two different

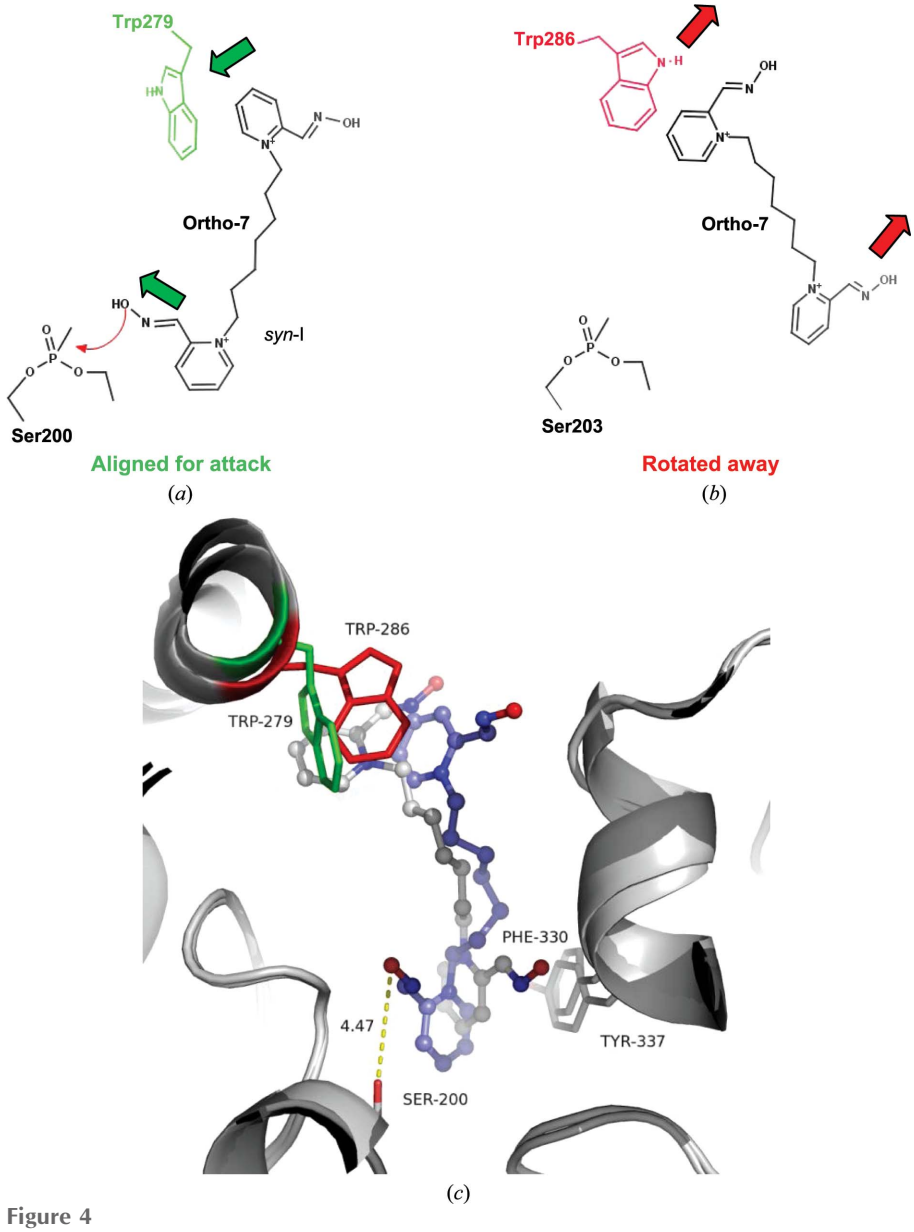

Figure 4
Comparison of the complexes of Ortho7–*Tc*AChE (PDB entry 5bwc) (oxime and Trp279 are colored blue and green) *versus* Ortho7-mouse AChE (PDB evtry 2gyv) (oxime and Trp286 are colored white and red) (*a*) In the *Tc*AChE structure the Ortho-7 oxime is directed towards the nucleophilic Ser200 and is aligned for nucleophilic attack. (*b*) In the mouse AChE structure the oxime at the bottom of the gorge is rotated away from the Ser203, and Trp286 packs face-to-face with the oxime at the top of the gorge. Trp286 undergoes a conformational change at the top of the gorge when the oxime is pointed away (PDB entry 2gyv) *versus* towards the active site serine (PDB entry 5bwc). A similar conformational change in Trp279 was observed in the 2BIM7–*Tc*AChE structure and the oxime was also rotated away from the Ser200 (PDB entry 5bwb). Within the gorge, there is a one residue difference: Phe330 (TcAChe) *versus* Tyr337 (mAChE) (shown as white sticks). The difference in hydrophobicity may account for the difference in the trapped conformation of the Ortho-7 oxime. The other residues in the gorge are identical and can be overlaid.

Table 2
K_i values of the oximes for *Tc*AChE and HuAChE.

Parameters were measured in duplicate.

Enzyme	Oxime	K_i (μ*M*)
*Tc*AChE	Ortho-7	0.061 ± 0.006
	2BIM-7	5 ± 1
HuAChE	Ortho-7	0.20 ± 0.06
	2BIM-7	35 ± 9

conformations when the bis-pyridinium oxime is bound to *Tc*AChE compared with mouse AChE (Fig. 3). Notably, the oxime conformation which may be more relevant to reactivation is found in the *Tc*AChE structure, *i.e.,* the oxime is well aligned for attack. In the mAChE–Ortho-7 structure the oxime group at the bottom of the gorge is rotated away from the active-site Ser (Fig. 4), and this was also seen in the 2BIM-7–*Tc*AChE structure (PDB entry 5bwb). The two AChE

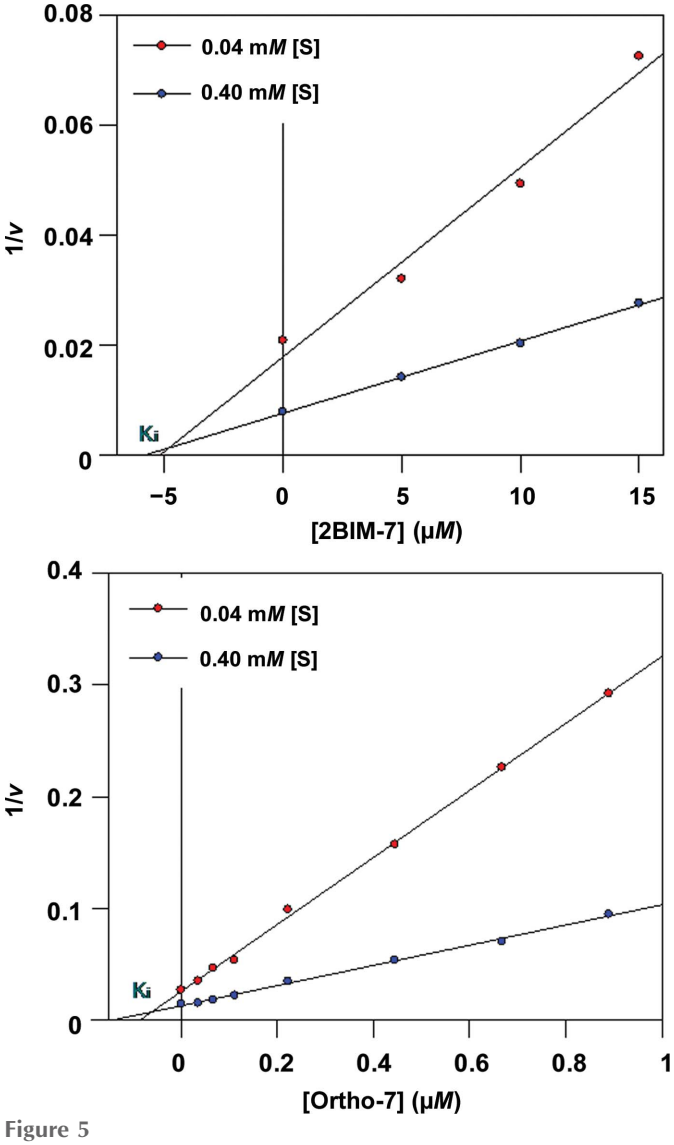

Figure 5
Measurement of the K_i values of Ortho-7 and 2BIM-7 with *Tc*AChE. The K_i of Ortho-7 was 0.06 μ*M* and the K_i of 2BIM-7 was significantly higher at 4.9 μ*M*.

Table 3
Kinetic parameters for reactivation of VX-inhibited and GB-inhibited human acetylcholinesterase.

Parameters were measured in duplicate.

Nerve-agent conjugate of huAChE	Oxime	K_d (μ*M*)	k_r (min^{-1})	$k_{r2} = k_r/K_d$ (mM^{-1} min^{-1})
huAChE–VX	2-PAM	120 ± 30	0.078 ± 0.006	0.6 ± 0.2
	2BIM-7	80 ± 20	0.15 ± 0.02	1.8 ± 0.5
	Ortho-7	0.17 ± 0.04	0.0091 ± 0.0004	50 ± 10
huAChE–GB	2-PAM	160 ± 10	0.185 ± 0.004	1.14 ± 0.08
	2BIM-7	260 ± 30	0.20 ± 0.01	0.76 ± 0.08
	Ortho-7	0.21 ± 0.07	0.0076 ± 0.0005	40 ± 10
huAChE–GA	2-PAM	71 ± 9	0.0045 ± 0.0001	0.064 ± 0.008
	2BIM-7	100 ± 30	0.0060 ± 0.0008	0.06 ± 0.02
	Ortho-7	0.17 ± 0.05	0.0082 ± 0.0006	50 ± 10

enzymes have one difference within the gorge-Phe330 in *Tc*AChE and Tyr337 in mAChE. Superposition of the 5bwc crystal structure with the solved native mouse AChE structure reveals a steric clash of Tyr337 with the superposed Ortho-7 oxime, suggesting that a conformational change of Tyr337, the oxime or both must occur upon binding mouse AChE (Supplementary Fig. S2). This difference could contribute to the approximately threefold difference in K_i values observed for TcAChE and human AChE (Table 2); human AChE, like mouse AChE, has Tyr instead of Phe at this position.

3.4. Kinetic parameters for 2BIM-7 and Ortho-7

To look for differences in the binding of the oxime to the free enzyme compared with the phosphylated enzyme, K_i and K_d values were measured. The kinetically determined dissociation constant of the oxime from the phosphylated enzyme, K_d, can be compared with the kinetically determined dissociation constant of the oxime from the free enzyme, K_i. Since K_d is determined from measured reactivation rates at varying concentrations of oxime, K_d reflects the binding of productively bound states (*i.e.*, bound aligned for attack in the phosphylated enzyme) which lead to reactivation as well as the binding of unproductively bound states which competitively inhibit. Within the narrow gorge, the alkyl groups of the organophosphate can affect the alignment of the oxime. For bis-oximes which interact with the PAS, allosteric effects may also affect the alignment of the oxime and reactivation rates.

The K_i value of Ortho-7 (0.06 μ*M*) for the free *Tc*AChE enzyme is 80-fold lower than that of 2BIM-7 (4.9 μ*M*), suggesting that the binding of the bis-imidazolium oxime, 2BIM-7, is relatively weak (Table 2, Fig. 5). In the 2BIM7–*Tc*AChE crystal structure the interaction of the oxime at the bottom of the gorge with Trp84 is not present (Fig. 1*f*); this may account for the weaker binding of the oxime to the free enzyme. Trp84 of the choline-binding pocket forms cation–π interactions with acetylcholine and edge-to-face interactions with Ortho-7 (Fig. 1*e*). The relatively tighter binding of Ortho-7 compared with 2BIM-7 applies to both human AChE and *Tc*AChE (Table 2). However, the dominant binding mode for Ortho-7 may differ among AChEs from different species, as suggested by our observation of an approximately threefold

difference in the apparent K_i values for human AChE *versus* *Tc*AChE (Table 2, Fig. 4).

The overall reactivation rate constant, $k_{r2} = k_r/K_d$, describes the efficiency of oxime reactivation for a given OP adduct. With regard to reactivation efficiency, 2BIM-7 was not significantly different from 2-PAM (Table 3). The highest k_{r2} values were observed with Ortho-7 and VX (k_{r2} = 50 mM^{-1} min^{-1}), GA (k_{r2} = 50 mM^{-1} min^{-1}) and GB (k_{r2} = 40 mM^{-1} min^{-1}). For comparison, the k_{r2} for HI-6 and VX is 21 mM^{-1} min^{-1} (Worek *et al.*, 2002), that for GA is 1 mM^{-1} min^{-1} (Cabal *et al.*, 2004) and that for GB is 6–13.5 mM^{-1} min^{-1} (Worek & Thiermann, 2013; Lundy *et al.*, 2011). The high k_{r2} values are predominantly owing to the tight binding of Ortho-7. Tight binding of oximes is not necessarily favorable, as many experimental oximes are toxic in animal models, *e.g.* the LD_{50} of the tight binding Ortho-7 is near 1 mg kg^{-1}, while the LD_{50} of the weaker binding 2-PAM oxime is 180 mg kg^{-1}, in mice (intramuscular delivery; Hammond *et al.*, 2003).

Ideally, the K_d should be lower than the K_i, as binding to the phosphylated enzyme is preferred compared with the free enzyme. For 2BIM-7, $K_d > K_i$ for all of the OPs tested, suggesting a degree of negative cooperativity (*i.e.*, enzyme phosphylation weakens the binding of the oxime). Since $K_d > K_i$ for 2BIM-7 (2.3–7.4-fold greater depending upon the OP), this suggests that not all bound states proceed to product formation; this is likely to be owing to the unproductively bound states such as that trapped in the crystal structure. For Ortho-7, the K_i values are comparable to the K_d values, suggesting that any unproductively bound states may be short-lived in the phosphylated enzyme.

4. Discussion

Organophosphate nerve agents and pesticides can cross the BBB to cause central nervous system damage, including intense seizure activity leading to death or long-term brain damage. Oral or intravenously administered oximes carrying a fixed positive charge (*i.e.* a quaternary amine), such as 2-PAM, do not efficiently cross the BBB (Mercey *et al.*, 2012; Sakurada *et al.*, 2003). Likewise, oxime moieties are highly reactive and have off-target effects and associated toxicities (Crook *et al.*, 1964; Bartosova *et al.*, 2006; Marrs, 1991). Several strategies to target oximes to the brain have been reviewed by Mercey *et al.* (2012), including the use of a P-glycoprotein inhibitor to achieve a twofold increase in HI-6 levels in the brain (Joosen *et al.*, 2011), the use of more lipophilic oximes (fluorinated oximes or lipophilic prodrugs, *e.g.* pro-2-PAM; Jeong, Kang *et al.*, 2009; Jeong, Park *et al.*, 2009; Shek *et al.*, 1976; DeMar *et al.*, 2010), the glycosylation of oximes (sugar-oximes) for entry *via* facilitative glucose transporters (Garcia *et al.*, 2010; Heldman *et al.*, 1986) and the use of neutral oximes such as monoisonitrosoacetone (MINA), diacetylmonooxime (DAM) and the imidazolium oximes (Kovarik *et al.*, 2013, 2015; Skovira *et al.*, 2010).

An oxime developed by De la Manche and coworkers almost 40 years ago [compound 1574, (carbaldoxime-4 pyridinium)-1-(methyl-1-imidazolium-3)-3-propane] carrying a pyridinium oxime and an imidazolium group was reported to have improved BBB permeability (De la Manche *et al.*, 1979). The incorporation of the oxime functionality into the imidazolium group in the *N*,*N*′-disubstituted imidazolium oxime ICD-467 produced a better reactivator of soman-inhibited cholinesterase than 2-PAM (Koplovitz & Stewart, 1988). However, ICD-467 was ineffective in reactivating AChE in the brain and was found to be toxic (Shih, 1993; Harris *et al.*, 1990). Imidazolium oximes can reactivate tabun-inhibited AChE (an adduct which contains a P—N bond instead of a P—O bond), and some can reactivate both tabun-inhibited and soman-inhibited AChE (RS150D, 70% reactivation of GA; Im2-2, 44% reactivation of GA; Im2-13, 20% reactivation of GA and 71% reactivation of GD; Kovarik *et al.*, 2013; Reiner & Simeon-Rudolf, 2006; Primožič *et al.*, 2004). None have been superior to the bispyridinium oximes in reactivating tabun-inhibited AChE (TMB-4, 91% reactivation of GA; obidoxime, 88% reactivation of GA; Worek *et al.*, 2012); however, TMB-4 is ineffective against GD (Inns & Leadbeater, 1983) and obidoxime is also a poor reactivator of GD-inhibited AChE (Worek *et al.*, 1998).

The experimental bis-imidazolium oxime, 2BIM-7, also incorporates the oxime functionality into an imidazolium group (Fig. 2), but unlike the *N*,*N*′-disubstituted imidazolium oximes, 2BIM-7, can be deprotonated to yield a neutral bis-oxime. Pyridinium oximes have limited BBB permeability owing to their fixed positively charged quaternary amines, whereas the N-substituted imidazolium oximes can be deprotonated and may cross the BBB un-ionized (Kovarik *et al.*, 2013). However, it is still unclear as to whether imidazolium oximes will have improved BBB permeability which can compensate for their moderate reactivation rates.

The experimental 2BIM-7 bis-imidazolium oxime that we describe here for the first time is a new type of bis-imidazolium oxime (Fig. 2) with comparable reactivating efficiency to 2-PAM (Table 3). The co-crystal structure revealed an unexpected result: sp^3 hybridization of one of the ring N atoms. This differs from the sp^2 hybridization of the pyridinium-ring N atom, which carries a fixed positive charge (quaternary amine) and has planar geometry (Supplementary Fig. S1). The tetrahedral geometry produced a sharp bend between the imidazolium ring and linker, and the bis-imidazolium oxime bound in an unproductive conformation. Most notably, 2BIM-7 induced a significant conformational change in the PAS, a key allosteric site (Figs. 1, 3 and 4). The *in vivo* significance of the enzyme conformational change is unknown; however, the PAS has been implicated in noncatalytic functions such as the nucleation of amyloid fibrils, cholinergic neuronal cell adhesion and neurite outgrowth (Johnson & Moore, 2006; Bourne *et al.*, 2003). Additionally, some isoforms of AChE interact with a range of extracellular matrix molecules during the development and repair of the neuromuscular junction (reviewed in Massoulié & Millard, 2009).

Drug-induced changes to the PAS conformation are also relevant to therapeutics for Alzheimer's disease (AD). Reversible inhibition of AChE catalysis has been examined as

a means to slow the progression of AD in some patients [Castro & Martinez, 2006; for example, using tacrine, donepezil (Aricept), galantamine (Razadyne), rivastigmine (Excelon) and huperzine]; these effects may also involve the physical disruption of amyloid formation (McGleenon *et al.*, 1999; Qian & Ke, 2014; Kurz, 1998; Zimmermann *et al.*, 2005). Propidium and donepezil, two anticholinesterase compounds which interact with the PAS, were previously found to inhibit human AChE-induced Aβ aggregation by 82 and 22%, respectively (Brocchieri & Karlin, 1994). The conformation of Trp279 in the propidium-bound complex is similar to that found in three of the four FDA-approved drugs for AD treatment [donepezil (PDB entry 1eve; Kryger *et al.*, 1999), galantamine (PDB entry 4ey6; Cheung *et al.*, 2012) and rivastigmine (PDB entry 1gqr; Bar-On *et al.*, 2002), but not tacrine (PDB entry 1acj; Harel *et al.*, 1993)] and is similar to that found in the inhibitor-free enzyme (PDB entry 1ea5; Dvir *et al.*, 2002) and two oxime-bound complexes [2-PAM (PDB entry 2vq6; M. Harel, I. Silman & J. L. Sussman, unpublished work) and Ortho7 (PDB entry 5bwc)]. It has been noted that there are no general rules for the design of AChE inhibitors that affect β-amyloid processing (Castro & Martinez, 2006), which suggests that other factors such as ligand-induced structural changes near to or far from the PAS or binding kinetics may be additional variables. Our data suggest that AChE from different species may be used to study the general trends of oxime binding and to link *in vitro* and *in crystallo* results, but also point to the need for high-resolution structural studies on human AChE that fully evaluate possible enzyme conformational changes of the PAS early in the drug-development cycle for compounds that are intended to be BBB-permeable.

Acknowledgements

This work was funded by the US Defense Threat Reduction Agency JSTO award E0036_08_WR_C to (CBM) and the Office of Naval Research/Naval Research Laboratory 6.1 base funding. The opinions or assertions contained herein belong to the authors and are not necessarily the official views of the US Army, the US Navy or the US Department of Defense.

References

Bar-On, P., Millard, C. B., Harel, M., Dvir, H., Enz, A., Sussman, J. L. & Silman, I. (2002). *Biochemistry*, **41**, 3555–3564
Bartosova, L., Kuca, K., Kunesova, G. & Jun, D. (2006). *Neurotox. Res.* **9**, 291–296.
Bourne, Y., Kolb, H. C., Radić, Z., Sharpless, K. B., Taylor, P. & Marchot, P. (2004). *Proc. Natl Acad. Sci. USA*, **101**, 1449–1454.
Bourne, Y., Taylor, P., Radić, Z. & Marchot, P. (2003). *EMBO J.* **22**, 1–12.
Broach, J., Krupa, R., Bird, S. B. & Manuell, M. E. (2014). *Am. J. Disaster Med.* **9**, 237–245.
Brocchieri, L. & Karlin, S. (1994). *Proc. Natl Acad. Sci. USA*, **91**, 9297–9301.
Brünger, A. T., Adams, P. D., Clore, G. M., DeLano, W. L., Gros, P., Grosse-Kunstleve, R. W., Jiang, J.-S., Kuszewski, J., Nilges, M., Pannu, N. S., Read, R. J., Rice, L. M., Simonson, T. & Warren, G. L. (1998). *Acta Cryst.* D**54**, 905–921.
Burda, A. M. & Sigg, T. (2001). *Am. J. Health Syst. Pharm.* **58**, 2274–2284.
Cabal, J., Kuca, K. & Kassa, J. (2004). *Pharmacol. Toxicol.* **95**, 81–86.
Castro, A. & Martinez, A. (2006). *Curr. Pharm. Des.* **12**, 4377–4387.
Cheung, J., Rudolph, M. J., Burshteyn, F., Cassidy, M. S., Gary, E. N., Love, J., Franklin, M. C. & Height, J. J. (2012). *J. Med. Chem.* **55**, 10282–10286.
Colletier, J.-P., Sanson, B., Nachon, F., Gabellieri, E., Fattorusso, C., Campiani, G. & Weik, M. (2006). *J. Am. Chem. Soc.* **128**, 4526–4527.
Crook, J. W., Cresthull, P., O'Neil, H. W. & Oberst, F. W. (1964). *Toxicol. Appl. Pharmacol.* **6**, 310–315.
De la Manche, I. S., Vergé, D. E., Bouchaud, C., Coq, H. & Sentenac-Roumanous, H. (1979). *Experientia*, **35**, 531–532.
DeMar, J. C. *et al.* (2010). *Chem. Biol. Interact.* **187**, 191–198.
Dvir, H., Jiang, H. L., Wong, D. M., Harel, M., Chetrit, M., He, X. C., Jin, G. Y., Yu, G. L., Tang, X. C., Silman, I., Bai, D. L. & Sussman, J. L. (2002). *Biochemistry*, **41**, 10810–10818.
Ekström, F., Pang, Y.-P., Boman, M., Artursson, E., Akfur, C. & Börjegren, S. (2006). *Biochem. Pharmacol.* **72**, 597–607.
Ellman, G. & Lysko, H. (1979). *Anal. Biochem.* **93**, 98–102.
Emsley, P. & Cowtan, K. (2004). *Acta Cryst.* D**60**, 2126–2132.
Garcia, G. E., Campbell, A. J., Olson, J., Moorad-Doctor, D. & Morthole, V. I. (2010). *Chem. Biol. Interact.* **187**, 199–206.
Gilson, M. K., Straatsma, T. P., McCammon, J. A., Ripoll, D. R., Faerman, C. H., Axelsen, P. H., Silman, I. & Sussman, J. L. (1994). *Science*, **263**, 1276–1278.
Hammond, P. I., Kern, C., Hong, F., Kollmeyer, T. M., Pang, Y.-P. & Brimijoin, S. (2003). *J. Pharmacol. Exp. Ther.* **307**, 190–196.
Harel, M., Schalk, I., Ehret-Sabatier, L., Bouet, F., Goeldner, M., Hirth, C., Axelsen, P. H., Silman, I. & Sussman, J. L. (1993). *Proc. Natl Acad. Sci. USA*, **90**, 9031–9035.
Harris, L. W., Anderson, D. R., Lennox, W. J., Woodard, C. L., Pastelak, A. M. & Vanderpool, B. A. (1990). *Biochem. Pharmacol.* **40**, 2677–2682.
Heldman, E., Ashani, Y., Raveh, L. & Rachaman, E. S. (1986). *Carbohydr. Res.* **151**, 337–347.
Inns, R. H. & Leadbeater, L. (1983). *J. Pharm. Pharmacol.* **35**, 427–433.
Jeong, H. C., Kang, N. S., Park, N.-J., Yum, E. K. & Jung, Y.-S. (2009). *Bioorg. Med. Chem. Lett.* **19**, 1214–1217.
Jeong, H. C., Park, N.-J., Chae, C. H., Musilek, K., Kassa, J., Kuca, K. & Jung, Y.-S. (2009). *Bioorg. Med. Chem.* **17**, 6213–6217.
Johnson, G. & Moore, S. W. (2006). *Curr. Pharm. Des.* **12**, 217–225.
Jokanović, M. (2012). *Curr. Top. Med. Chem.* **12**, 1775–1789.
Jokanović, M. & Prostran, M. (2009). *Curr. Med. Chem.* **16**, 2177–2188.
Joosen, M. J. A. van der, van Schans, M. J., Dijk, C. G. M., Kuijpers, W. C., van Wortelboer, H. M. & Helden, H. P. M. (2011). *Toxicol. Lett.* **206**, 67–71.
Koplovitz, I. & Stewart, J. R. (1988). *Novel Imidazolium Oximes as Improved Nerve Agent Antidotes.* USAMRICD-TR-88-06 (AD# A198242). Fort Detrick: US Army Medical Research Institute of Chemical Defense.
Kovarik, Z., Maček Hrvat, N., Katalinic, M., Sit, R. K., Paradyse, A., Žunec, S., Musilek, K., Fokin, V. V., Taylor, P. & Radić, Z. (2015). *Chem. Res. Toxicol.* **28**, 1036–1044.
Kovarik, Z., Maček, N., Sit, R. K., Radić, Z., Fokin, V. V., Sharpless, K. B. & Taylor, P. (2013). *Chem. Biol. Interact.* **203**, 77–80.
Kurz, A. (1998). *J. Neural Transm. Suppl.* **54**, 295–299.
Kryger, G., Silman, I. & Sussman, J. L. (1999). *Structure Fold. Des.* **7**, 297–307.
Lundy, P. M., Hamilton, M. G., Sawyer, T. W. & Mikler, J. (2011). *Toxicology*, **285**, 90–96.
Luo, C., Chambers, C., Pattabiraman, N., Tong, M., Tipparaju, P. & Saxena, A. (2010). *Biochem. Pharmacol.* **80**, 1427–1436.
Marrs, T. C. (1991). *Adverse Drug React. Toxicol. Rev.* **10**, 61–73.
Massoulié, J. & Millard, C. B. (2009). *Curr. Opin. Pharmacol.* **9**, 316–325.

McGleenon, B. M., Dynan, K. B. & Passmore, A. P. (1999). *Br. J. Clin. Pharmacol.* **48**, 471–480.
Mercey, G., Verdelet, T., Renou, J., Kliachyna, M., Baati, R., Nachon, F., Jean, L. & Renard, P.-Y. (2012). *Acc. Chem. Res.* **45**, 756–766.
Millard, C. B., Kryger, G., Ordentlich, A., Greenblatt, H. M., Harel, M., Raves, M. L., Segall, Y., Barak, D., Shafferman, A., Silman, I. & Sussman, J. L. (1999). *Biochemistry*, **38**, 7032–7039.
Nardini, M. & Dijkstra, B. W. (1999). *Curr. Opin. Struct. Biol.* **9**, 732–737.
Navaza, J. (2001). *Acta Cryst.* D**57**, 1367–1372.
Pang, Y.-P., Kollmeyer, T. M., Hong, F., Lee, J.-C., Hammond, P. I., Haugabouk, S. P. & Brimijoin, S. (2003). *Chem. Biol.* **10**, 491–502.
Primožič, I., Odžak, R., Tomić, S., Simeon-Rudolf, V. & Reiner, E. (2004). *J. Med. Chem. Def.* **2**, 1–30.
Qian, Z. M. & Ke, Y. (2014). *Front. Aging Neurosci.* **6**, 216.
Raves, M. L., Harel, M., Pang, Y.-P., Silman, I., Kozikowski, A. P. & Sussman, J. L. (1997). *Nature Struct. Biol.* **4**, 57–63.
Reiner, E. & Simeon-Rudolf, V. (2006). *Arh. Hig. Rada Toksikol.* **57**, 171–179.
Rydberg, E. H., Brumshtein, B., Greenblatt, H. M., Wong, D. M., Shaya, D., Williams, L. D., Carlier, P. R., Pang, Y.-P., Silman, I. & Sussman, J. L. (2006). *J. Med. Chem.* **49**, 5491–5500.
Sakurada, K., Matsubara, K., Shimizu, K., Shiono, H., Seto, Y., Tsuge, K., Yoshino, M., Sakai, I., Mukoyama, H. & Takatori, T. (2003). *Neurochem. Res.* **28**, 1401–1407.
Sanson, B., Colletier, J.-P., Xu, Y., Lang, P. T., Jiang, H., Silman, I., Sussman, J. L. & Weik, M. (2011). *Protein Sci.* **20**, 1114–1118.
Schüttelkopf, A. W. & van Aalten, D. M. F. (2004). *Acta Cryst.* D**60**, 1355–1363.
Shek, E., Higuchi, T. & Bodor, N. (1976). *J. Med. Chem.* **19**, 108–112.
Shih, T.-M. (1993). *Arch. Toxicol.* **67**, 637–646.
Skovira, J. W., O'Donnell, J. C., Koplovitz, I., Kan, R. K., McDonough, J. H. & Shih, T.-M. (2010). *Chem. Biol. Interact.* **187**, 318–324.
Steinberg, G. M., Lieske, C. N., Boldt, R., Goan, J. C. & Podall, H. E. (1970). *J. Med. Chem.* **13**, 435–446.
Stojiljković, M. P. & Jokanović, M. (2006). *Arh. Hig. Rada Toksikol.* **57**, 435–443.
Sussman, J. L., Harel, M., Frolow, F., Oefner, C., Goldman, A., Toker, L. & Silman, I. (1991). *Science*, **253**, 872–879.
Sussman, J. L., Harel, M., Frolow, F., Varon, L., Toker, L., Futerman, A. H. & Silman, I. (1988). *J. Mol. Biol.* **203**, 821–823.
Sussman, J. L., Harel, M. & Silman, I. (1993). *Chem. Biol. Interact.* **87**, 187–197.
Wandhammer, M., de Koning, M., van Grol, M., Loiodice, M., Saurel, L., Noort, D., Goeldner, M. & Nachon, F. (2013). *Chem. Biol. Interact.* **203**, 19–23.
Wang, E. I. C. & Braid, P. E. (1967). *J. Biol. Chem.* **242**, 2683–2687.
Wilson, I. B. & Ginsburg, B. (1955). *Biochim. Biophys. Acta*, **18**, 168–170.
Winn, M. D. *et al.* (2011). *Acta Cryst.* D**67**, 235–242.
Worek, F., Reiter, G., Eyer, P. & Szinicz, L. (2002). *Arch. Toxicol.* **76**, 523–529.
Worek, F. & Thiermann, H. (2013). *Pharmacol. Ther.* **139**, 249–259.
Worek, F., Widmann, R., Knopff, O. & Szinicz, L. (1998). *Arch. Toxicol.* **72**, 237–243.
Worek, F., Wille, T., Koller, M. & Thiermann, H. (2012). *Biochem. Pharmacol.* **83**, 1700–1706.
Zimmermann, M., Borroni, B., Cattabeni, F., Padovani, A. & Di Luca, M. (2005). *Neurobiol. Dis.* **19**, 237–242.